 FDMP, vol.9, no.3, pp.267-290, 2013

Convective Film Condensation in an Inclined Channel with Porous Layer

Lazhar Merouani[1], Belkacem Zeghmati[2] and Azeddine Belhamri[3]

Abstract: The present work is a numerical study of laminar film condensation from vapor-gas mixtures in an inclined channel with an insulated upper wall and an isothermal lower wall coated with a thin porous material. A two-dimensional model is developed using a set of complete boundary layer equations for the liquid film and the steam-air mixture while the Darcy-Brinkman-Forchheimer approach is used for the porous material. The governing equations are discretized with an implicit finite difference scheme. The resulting systems of algebraic equations are numerically solved using Gauss and Thomas algorithms. The numerical results enable to determine the velocity, temperature and vapor concentration profiles in the steam-air mixture, the liquid film and the porous substrate. The axial evolution of the condensate flow rate and the wall heat flux are also presented and analyzed for different operating conditions. It is found that the inclination angle, the inlet values of relative humidity and the Reynolds number exert an influence on the condensation process much more significant than that coming from a change in the porous layer properties.

Keywords: Condensation, forced convection, liquid film, porous material, steam-air mixture.

1 Introduction

Heat and mass transfer problems in porous materials have received increasing attention because of their practical relevance to industry and a variety of other fields (heat exchangers, chemical reactors, soil pollution and geothermal applications). Much literature exists on the case of convection in homogeneous fluids (Lappa (2004, 2005, 2007a,b, 2011, 2013) and references therein). Similarly, many theoretical and experimental studies have been performed on the convective flows in

[1] Department of Science and Technology, University of Abbes Laghrour of Khenchela, Algeria
[2] Laboratoire de Mathématiques et de Physique LAMPS, Univerité de Perpignan, France
[3] Laboratory of Climatic Engineering, University of Mentouri of Constantine, Algeria

porous media. A general summary of these works can be found for instance in Kaviany (1991); Bories and Prat (1995); Nield and Bejan (1998). More recent analyses are due to Choukairy and Bennacer (2012); Hamimid, Guellal, Amroune, and Zeraibi (2012); Al-Ajmi and Mosaad (2012); Ram and Bhandari (2012); Labed, Bennamoun, and Fohr (2012).

In particular, the specific problem of laminar film condensation within thin porous coatings was first introduced by Renken, Soltykiwicz, and Poulikakos (1989) for the enhancement of condensation heat transfer. Shekarriz and Plumb (1989) showed that the presence of porous fins on the external wall of a horizontal tube contributes to reduce significantly the thickness of the liquid film and thus to improve the heat transfer at the wall. Experimental and numerical studies of pure steam condensation by forced convection on inclined plates coated with a thin porous permeable layer were then conducted by Renken, Carneiro, and Meechan (1994); Renken and Raich (1996). These authors found a significant increase in heat transfer coefficients compared to those of an ordinary uncoated surface for the same thermophysical conditions. They also showed that the thermal dispersion effect leads to a significant increase of the heat transfer rate and it becomes more pronounced as the Reynolds number increases.

Ma and Wang (1998) presented a mathematical model for the laminar film condensation of pure steam on a porous coated surface based on the dispersion effect in the porous coating, using the Darcy-Brinkman simplified model. They showed that the condensate film thickness and the local Nusselt number increase with the thickness of the porous coating. However, they found discrepancies between numerical results and experimental data, which may result from the effect of non-condensable gas in the experiments.

A numerical investigation of a problem of steam condensation in a thin porous layer was also performed by Asbik, Chaynane, Boushaba, Zeghmati, and Khmou (2003). In their study the transfer equations in the porous region are obtained in the framework of the Darcy-Brinkman-Forchheimer model. The analytical results are presented for velocity and temperature profiles in the porous layer, the liquid film thickness, the local Nusselt number and the influence of Reynolds and Darcy numbers.

A theoretical model of vapor condensation on a porous flat plate was presented by Chaynane, Asbik, Boushaba, Zeghmati, and Khmou (2004). A significant augmentation of the heat transfer rate was found while the absence of the inertial term in the liquid transfer equation causes an increase of the liquid film thickness.

An analytical solution for the film condensation by natural convection within a saturated porous layer was developed by Asbik, Zeghmati, Gualous-Louahlia, and Yan

(2007). It was found that the thermal dispersion has a significant effect on the heat transfer enhancement. Moreover, a numerical study of laminar vapor condensation along a porous wall was presented later by El-Hammami, Feddaoui, Mediouni, Mir, and Mir (2010). The simulation results show the effects of the inlet values of temperature, pressure, Reynolds number and the porous layer thickness on the heat and mass transfer performance.

All the above studies are restricted to the case of pure isothermal steam without considering transfers in the vapor phase. So, the objective of this paper is to study the problem of laminar film condensation of a vapor flowing in the presence of non-condensable gas in an inclined channel with a lower wall coated with a thin porous layer. A more accurate approach is developed to improve previous models taking into account the coupled transfers in the three regions: porous layer, liquid film and vapor-gas mixture. The Darcy-Brinkman-Forchheimer model is used for the fluid flow in the porous medium. Transfers in the steam-air mixture and the liquid film are described by a set of complete boundary layer equations. The study is conducted for wide ranges of the governing parameters taking into account the inertia and convection terms, the axial pressure gradient, the shear stresses at the liquid-steam/air mixture and at the liquid-porous layer interfaces.

2 Physical model

The physical configuration under consideration is shown schematically in Fig. 1a. It is composed of two parallel plates separated by a distance R and inclined at an angle θ from the horizontal. The upper wall is insulated while the lower wall is coated with a thin porous layer of thickness H. A mixture of steam and non-condensable gas enters the channel with uniform values of velocity, temperature, pressure and vapor mass fraction. During the flow, vapor condensation occurs on the lower plate creating three distinct regions in the channel: the saturated porous coating, the condensate liquid film and the vapor-gas mixture. A Cartesian coordinates system (Oxy) is chosen as shown in Fig. 1a and the following assumptions are made:

- Fluid flows are steady, laminar and two-dimensional,
- Boundary layer approximations are valid for the liquid film and the mixture,
- The vapor-gas mixture is composed of two ideal gases,
- The pressure is uniform in the y direction,
- The saturated porous coating is completely covered by the condensate from the channel inlet,

- Viscous dissipation, radiative heat transfer, Dufour and Soret effects are negligible.

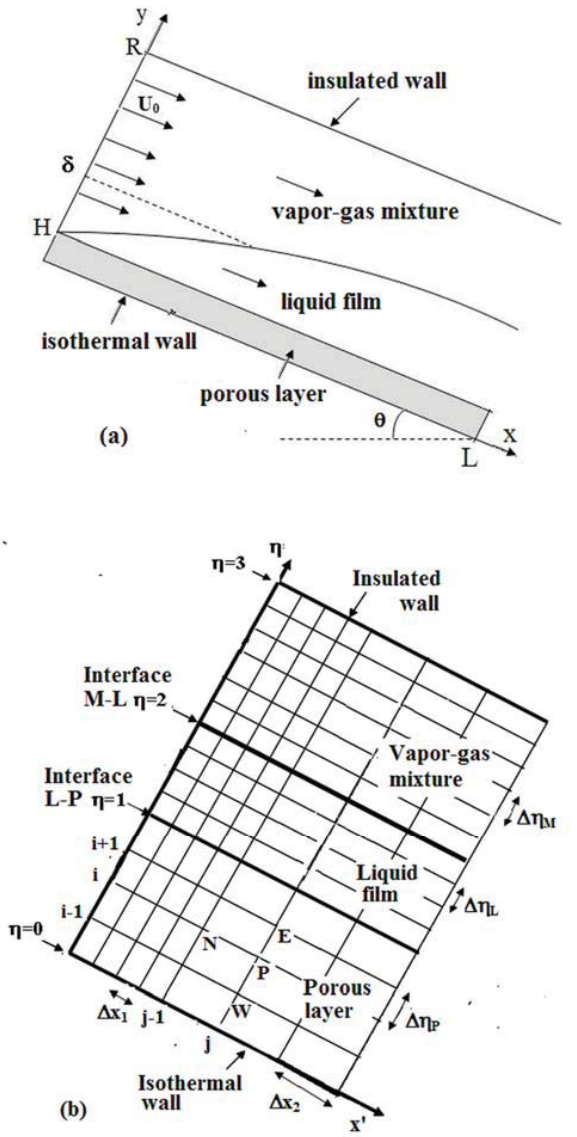

Figure 1: Schematic representation (a) Physical model and coordinate system (b) Numerical domain and discretization grid

3 Governing equations

Since the film thickness $\delta - H$ varies along the wall, the following coordinate transformation is applied:

$$\eta_p = \frac{y}{H}, \eta_L = 1 + \frac{y-H}{\delta - H}, \eta_M = 2 + \frac{y-\delta}{R-\delta}, x' = x \tag{1a-d}$$

This transformation leads to additional terms in the governing equations but enables to define clearly the liquid-mixture interface along the solution domain. The positions of the lower wall, the liquid-porous layer interface, the liquid-mixture interface and the upper wall are respectively defined by $\eta = 0, 1, 2, 3$ (Fig. 1b).

Transfers in the liquid film and the mixture are governed by mass, momentum, energy and diffusion equations. In the porous layer, the fluid flow is described by the Darcy-Brinkman-Forchheimer model including the influence of viscous effects, flow inertia and pressure gradient. Due to the above assumptions, the governing equations are written for each phase as follows:

- Continuity equations:

$$\frac{\partial U_p}{\partial x'} + \frac{1}{H}\frac{\partial V_p}{\partial \eta_p} = 0 \tag{2}$$

$$\frac{\partial U_L}{\partial x'} + \frac{\delta'(1-\eta_L)}{(\delta - H)}\frac{\partial U_L}{\partial \eta_L} + \frac{1}{(\delta - H)}\frac{\partial V_L}{\partial \eta_L} = 0 \tag{3}$$

$$\frac{\partial U_M}{\partial x'} + \frac{\delta'(\eta_M - 3)}{(R-\delta)}\frac{\partial U_M}{\partial \eta_M} + \frac{1}{(R-\delta)}\frac{\partial V_M}{\partial \eta_M} = 0 \tag{4}$$

where

$$\delta' = d\delta/dx \tag{5}$$

- Momentum, energy and mass diffusion equations:

$$U_p \frac{\partial \psi_p}{\partial x'} + \frac{V_p}{H}\frac{\partial \psi_p}{\partial \eta_k} = \frac{\Gamma_{\psi_p}}{H^2}\frac{\partial^2 \psi_p}{\partial \eta_p^2} + S_{\psi_p} \tag{6}$$

$$U_L \frac{\partial \psi_L}{\partial x'} + \left(\frac{\delta' U_L(1-\eta_L) + V_L}{(\delta - H)}\right)\frac{\partial \psi_L}{\partial \eta_L} = \frac{\Gamma_{\psi_L}}{(\delta - H)^2}\frac{\partial^2 \psi_L}{\partial \eta_L^2} + S_{\psi_L} \tag{7}$$

$$U_M \frac{\partial \psi_M}{\partial x'} + \left(\frac{\delta' U_M(\eta_M - 3) + V_M}{(R-\delta)}\right)\frac{\partial \psi_M}{\partial \eta_M} = \frac{\Gamma_{\psi_M}}{(R-\delta)^2}\frac{\partial^2 \psi_M}{\partial \eta_M^2} + S_{\psi_M} \tag{8}$$

where $\psi_k = (U_k, T_k, C)$, Γ_{ψ_k} are the diffusion coefficients and S_{ψ_k} are the source terms for each phase. Expressions of Γ_{ψ_k}, S_{ψ_k} are reported in Table 1.

Table 1: List of coefficients Γ_{ψ_k} and terms S_{ψ_k} in transfer equations (6-8)

Equation	ψ_k	Γ_{ψ_k}	S_{ψ_k}
Momentum	U_p	$\mu_e^* \varepsilon^2 \upsilon_L$	$\frac{-\varepsilon^2}{\rho_L}\frac{dP}{dx} + \varepsilon^2 g.\sin\theta$
($k = P, L, M$)			$-\varepsilon^2 \upsilon_L U_p K^{-1} - \varepsilon^2 F U_p^2 K^{-1/2}$
	U_L	υ_L	$g.\sin\theta - \frac{1}{\rho_L}\frac{dP}{dx}$
	U_M	υ_M	$g.\sin\theta - \frac{1}{\rho_M}\frac{dP}{dx}$
Equation	T_p	$\lambda_e^* \alpha_L$	0
	T_L	α_L	0
	T_M	α_M	$\frac{D_v(c_{pv}-c_{pa})}{c_{pM}(R-\delta)^2}\frac{\partial T_M}{\partial \eta_M}\frac{\partial C}{\partial \eta_M}$
Mass diffusion	C	D_v	0
($k = M$)			

- Mass flow rate equations:

$$\int_0^1 H\rho_L U_p \, d\eta_p + \int_1^2 (\delta - H)\rho_L U_L \, d\eta_L + \int_2^3 (R-\delta)\rho_M U_M \, d\eta_M = q_0 \tag{9a}$$

$$q_C = \int_0^x J_v \, dx \tag{9b}$$

where q_C is the flow rate produced by condensation along the lower wall and q_0 the inlet flow rate per unit width.

The boundary conditions for equations (2-8) are:

- At the channel inlet ($x = 0$), velocity, pressure, temperature and vapor concentration of the steam-gas mixture are assumed uniform:

$$U_M = U_0, T_M = T_0, C = C_0, P = P_0 \tag{10a-d}$$

- At the lower plate ($\eta = 0$), no slip and constant temperature are imposed:

$$U_p = 0, \tag{11a}$$

$$T_p = T_w \tag{11b}$$

- At the interface between liquid and porous layer ($\eta = 1$), continuity of velocity, shear stress, temperature and heat flux are imposed:

$$U_L = U_p, \tag{12a}$$

$$\frac{\mu_L}{(\delta - H)} \frac{\partial U_L}{\partial \eta_L} = \frac{\mu_e}{H} \frac{\partial U_p}{\partial \eta_p} \tag{12b}$$

$$T_L = T_p, \tag{13a}$$

$$\frac{\lambda_L}{(\delta - H)} \frac{\partial T_L}{\partial \eta_L} = \frac{\lambda_e}{H} \frac{\partial T_p}{\partial \eta_p} \tag{13b}$$

- At the interface between liquid and steam-air mixture ($\eta = 2$), equations of both phases are connected by the continuity conditions:

$$U_L = U_M, \tag{14a}$$

$$\frac{\mu_L}{(\delta - H)} \frac{\partial U_L}{\partial \eta_L} = \frac{\mu_M}{(R - \delta)} \frac{\partial U_M}{\partial \eta_M} \tag{14b}$$

$$T_L = T_M, \tag{15a}$$

$$-\frac{\lambda_L}{(\delta - H)} \frac{\partial T_L}{\partial \eta_L} = J_v L_c - \frac{\lambda_M}{(R - \delta)} \frac{\partial T_M}{\partial \eta_M} \tag{15b}$$

$$J_v = \rho_L (V_L + U_L \delta')_i = \rho_M (V_M + U_M \delta')_i \tag{16a-b}$$

The saturated vapor concentration is calculated using the following relation:

$$C_i = \frac{\gamma P_{vs}(T_i)}{(\gamma - 1) P_{vs}(T_i) + P_i} \tag{17}$$

The Bertrand's relation is used to calculate the partial pressure of the saturated vapor P_{vs} (in bars):

$$\log_{10}(P_{vs}) = 17.443 - 2795/T_i - 3.868 \times \log_{10}(T_i) \tag{18}$$

- At the upper plate ($\eta = 3$), no-slip conditions, insulated and impermeable wall are considered:

$$U_M = 0, \frac{\partial T_M}{\partial \eta_M} = 0, \frac{\partial C}{\partial \eta_M = 0} \tag{19a-c}$$

The equations (2-9) and the boundary conditions (10-19) are then adimensionalized by using the following reduced variables:

$$(x^*, \delta^*) = \frac{(x, \delta)}{R}, (U_k^*, V_k^*) = \frac{(U_k, V_k)}{\sqrt{gR}}, \tag{20a-b}$$

$$T_k^* = \frac{T_k - T_w}{T_0 - T_w}, P^* = \frac{P - P_0}{\rho_0 g R}, q_k^* = \frac{q_k}{\mu_L} \tag{20c-e}$$

As a result, the following non-dimensional parameters appear in the transformed equations:

$$Da = K/R^2, H^* = H/R, \gamma = M_v/M_a, \tag{21a-c}$$

$$Re_0 = U_0(R-H)/\upsilon_0, \mu_e^* = \mu_e/\mu_L, \lambda_e^* = \lambda_e/\lambda_L \tag{21d-f}$$

Moreover, the local Nusselt number Nu at the lower plate and the overall heat flux ϕ^* generated by the condensation process are defined below:

$$Nu = \left(\frac{R\lambda_e^*}{(T_0 - T_w)H} \frac{\partial T_p}{\partial \eta_p} \right)_w, \tag{22a}$$

$$\phi^* = \int_0^{x^*} Nu.dx^* \tag{22b}$$

4 Numerical procedure

The dimensionless equations are discretized on a Cartesian structured grid using an implicit finite difference method. Fig. 1b represents the numerical mesh with three space steps $\Delta\eta_p$, $\Delta\eta_L$, $\Delta\eta_M$ in each domain (porous layer, liquid film, mixture). Each grid node is characterized by two integers i, j representing its transverse and axial coordinates. The mesh is refined in the entrance zone where the first axial space step Δx_1 is relatively fine on a length for which j varies from 0 to M'. Beyond this distance, we use a coarser grid where Δx_2 is significantly greater than Δx_1 and j varies from M' to M. The derivatives are approximated using the central differences for internal nodes, and backward or forward differences of second order for boundary conditions. The discretization process leads to algebraic equations that can be written as follows:

$$a_W \psi(W) + a_P \psi(P) + a_E \psi(E) + a_N \psi(N) = s_{\psi_k}(P) \tag{23}$$

where a_W, a_E, a_P, a_N are the coefficients of the variables $\psi = (U_k^*, T_k^*, C)$ at the nodes W, E, P, N (Fig. 1b). These non-linear equations are solved by Gauss and

Thomas algorithms using an iterative method and a transverse line by line procedure. Moreover, under-relaxation coefficients are used to enable smooth evolutions of variables between two successive iterations:

$$\psi_{p,new} = \psi_p^{'} + \alpha(\psi_p - \psi_p^{'}) \tag{24}$$

where $\psi_p^{'}$ represents the value of ψ_p at the previous iteration. In this work, the following values of the under-relaxation factors α are used:

- $\alpha = 0.4$ for axial velocity, pressure gradient, temperature, vapor mass fraction,
- $\alpha = 0.2$ for transverse velocity.

At each axial position, the convergence of the iterative process is supposed achieved when the following criterion between two successive iterations $(K-1)$ and (K) is verified for all variables:

$$\max \left| \frac{\psi^K(i,j) - \psi^{K-1}(i,j)}{\psi^K(i,j)} \right| < 10^{-5} \tag{25}$$

5 Solution algorithm

A computer code was developed to implement the numerical procedure described above. Calculations are performed line by line according to the following steps:

1. At the inlet of the channel, initial values of mixture parameters are given and physical properties of fluids are calculated.
2. An arbitrary value δ_1 of the condensate thickness is imposed at the current location j.
3. The momentum equations in the three phases associated with the overall mass conservation are solved using the Gauss algorithm to obtain the velocity field and the axial pressure gradient.
4. The values of transverse velocity are calculated from the continuity equation in the three media.
5. The equations of energy in the three media and mass diffusion in the mixture are solved using the Thomas algorithm, to obtain the temperature and the vapor mass fraction fields.

6. If the criterion (25) is verified for all nodes in the line j, then we move to the next step. Otherwise, steps 3-6 are repeated.

7. A second arbitrary value δ_2 of the condensate thickness is imposed ($\delta_2 \neq \delta_1$). Steps 3-6 are repeated until the criterion (25) is verified.

8. The relative error E of the liquid flow rate is calculated:

$$E = 1 - \frac{q_L + q_P}{q_C} \tag{26}$$

If $|E| > 10^{-5}$, then a better value of δ is calculated by the secant method:

$$\delta_{it} = \delta_{it-1} - E_{it-1}\left(\frac{\delta_{it-1} - \delta_{it-2}}{E_{it-1} - E_{it-2}}\right) \tag{27}$$

where it is the iteration number and steps 3-6 are repeated until the criterion (25) is verified. Otherwise, the last value of δ is retained and we move to the next line.

9. The physical properties of fluids are revalued from the interface temperature and mass fraction values obtained in the previous line.

10. Steps 2-8 are repeated for the new line until convergence.

11. The calculations are stopped when the end of the channel is reached.

6 Validation of the numerical model

The computer code was validated by comparison with the most clearly related numerical solutions of Siow (2001) for a forced convection condensation of a saturated steam-ai in a horizontal channel with non-porous walls. Calculations are performed for $Re_0 = 1000$, $P_0 = 1atm$, $C_0 = 0.9$. Fig. 2 shows the dimensionless thickness of the liquid film for two values of the temperature difference ($T_0 - T_w = 5, 10°C$). As it can be seen, there is a good agreement between our results and those of Siow since the discrepancies are less than 3%.

Moreover, the influence of the mesh size on the average Nusselt number Nu_m was also analyzed. Several grid sizes were tested for typical conditions (indicated in the next section). We noted that an increase of the grid size from (2500×48) to(5125×96) leads to a maximum variation of Nu_m about 4%. As the relative error obtained with the grid $(M^{'}, M) = (1000, 2500)$, $(N_P, N_L, N_M) = (10, 10, 40)$ was within 1% compared to the finest mesh, it was considered sufficiently accurate. Thus, all calculations presented in this work have been performed using this grid.

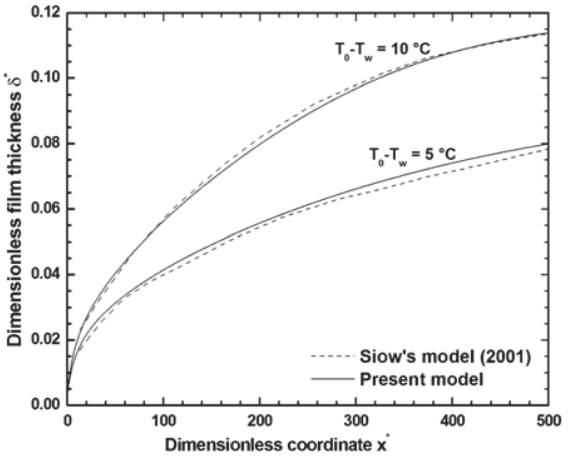

Figure 2: Axial evolution of film thickness in a horizontal channel with non-porous walls. Comparison with results of Siow (2001)

7 Results and discussion

Calculations are firstly conducted for the following typical conditions:

- channel: $L = 3m$, $R = 1cm$, $\theta = 5^\circ$,
- vapor-gas mixture: $P_0 = 1atm$, $T_0 = 98.2^\circ C$, $\varphi_0 = 1$, $C_0 = 0.9$, $Re_0 = 700$,
- porous layer: $\Delta T = 10^\circ C$, $H^* = 0.01$, $Da = 10^{-4}$, $\lambda_e^* = 1$, $\mu_e^* = 1$.

Results are presented as:

- local profiles of velocity, temperature and vapor mass fraction for various axial positions,
- axial evolutions of the liquid mass flow rate and the heat flux on the lower wall.

The end of condensation is considered achieved when all the axial flow parameters become steady along the channel.

7.1 Local field profiles

Fig. 3a shows the axial velocity profiles at different axial positions x^* varying from 1 to 300 in the three media. At the inlet of the system, a vapor-gas mixture enters

the channel with uniform velocity and a high vapor concentration. A liquid film condensation occurs in the cooled porous layer. Because of its small thickness and high inlet condensation rate, it is completely covered by the liquid condensate. In the mixture region, velocity profiles decrease quickly near the leading edge, resulting in high velocity gradients along the walls. They are progressively deformed under the effect of steam removal along the flow and are described from a distance $x^* = 5$ by quasi parabolic profiles with a maximum value near the middle of the channel. Then, they still decrease and become practically invariant from a distance $x^* = 250$.

In the liquid film and the porous layer, the velocity values of the condensate increase progressively along the flow under the effect of gravity and shear stresses at the interfaces. The condensate velocity in the porous layer remains significantly lower than that of the liquid film. At the liquid-porous layer and liquid-mixture interfaces, the limit values of velocity are respectively $U^* = 0.75, 0.162$ reached in steady state. In the three phases, the velocity profiles have no significant difference from $x^* = 250$ corresponding to the end of condensation.

Fig. 3b and 3c represent the temperature and vapor concentration profiles at the same axial positions. The temperature of the lower wall is maintained constant T_W. At the channel inlet, temperature and vapor mass fraction of the mixture are supposed uniform. They decrease suddenly at the porous layer interface and more slowly in the mixture. The maximum values of temperature and vapor concentration are found on the upper wall assumed adiabatic and impermeable and decrease up to the interface between liquid and steam-air mixture with imposed saturation conditions. In the liquid film and the porous layer, temperature variations are smaller and their profiles are quasi linear, due to the negligible effect of convective terms in the energy equations of these media. In the three phases, the profiles tend progressively to uniform values corresponding to isothermal saturation at the prescribed wall conditions reached at the end of condensation. A residual quantity of steam corresponding to saturation at the wall temperature remains in the mixture ($C_f = 0.53$)

7.2 Axial evolutions of flow parameters

Fig. 4 shows the axial variation of the condensate mass flow rate at the cooled wall. As it can be seen, the increase of flow rate has a large axial slope near the leading edge. This evolution is due to the important vapor concentration gradient leading to a simultaneous increase of the film thickness and the liquid velocity. After a long distance from the inlet ($x^* = 250$), it tends asymptotically to its limit value corresponding to the end of condensation process.

Fig. 4 shows also the evolution of the heat flux transferred to the lower wall. This

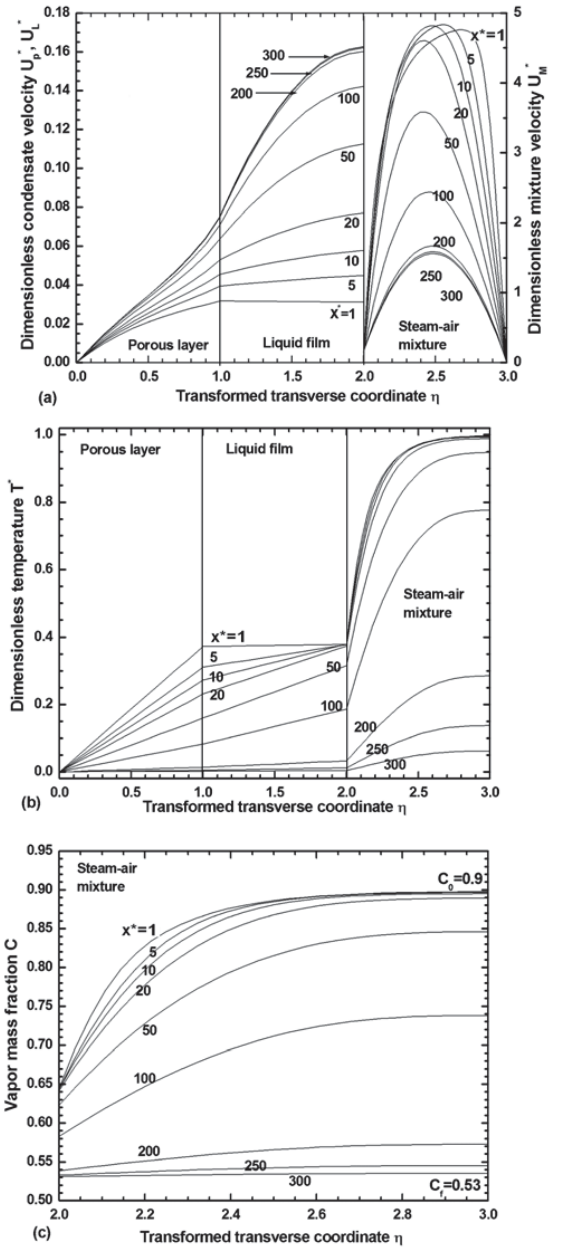

Figure 3: Local dimensionless profiles at various sections: (a) velocity, (b) temperature, (c) vapor concentration

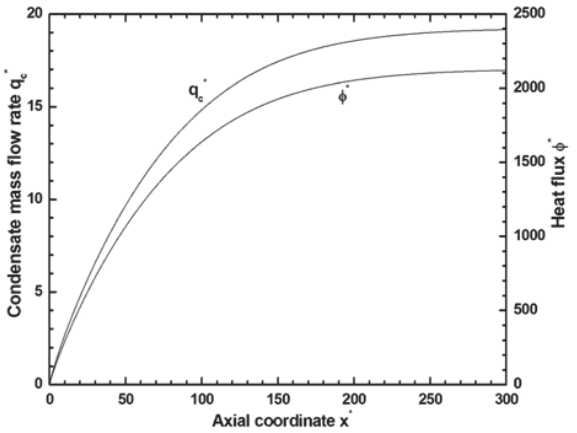

Figure 4: Axial evolutions of condensate mass flow rate and heat flux at the lower wall

heat transfer is closely related to the thermal gradients in the porous layer which are very large in the inlet region leading to high heat flux. Indeed, we find that half of the total heat flux is transmitted over a very short distance in the entrance region ($x^* < 50$). In the porous layer, the interface temperature and the thermal gradients decrease along the flow, resulting in a significant reduction in heat flux. Moreover, as the upper wall is adiabatic, the heat flux is fully transmitted to the lower wall across the liquid film and the porous layer, resulting from both the latent heat of condensation and the sensible cooling of the mixture. At the exit of the channel, the end of condensation is practically reached. Heat and mass transfer processes tend to disappear because the whole system approaches progressively an uniform temperature T_w and the mixture has also a uniform vapor concentration corresponding to the final saturation C_f.

7.3 Effect of the operating conditions

The effects of various operating conditions on the condensation process are also examined. All the results presented here concern the evolutions of the condensate flow rate and the heat flux along the condensation path.

7.3.1 Effect of the inlet Reynolds number

Fig. 5 shows the effect of Re_0 on the evolutions of the condensate flow rate and the heat flux for $P_0 = 1atm$, $T_0 = 98.2°C$, $\Delta T = 10°C$, $\theta = 5°$. Calculations are performed for Re0 varying between 350 and 1300 corresponding to a laminar flow.

As the wall temperature T_w is maintained constant, the final vapor concentration of the mixture has the same value $C_f = 0.53$, representing the mass fraction of the non-condensed vapor in all cases. The inlet steam flow rate increases with Re_0 leading to higher condensation rate. It follows a significant enhancement in the liquid flow rate and the film thickness.

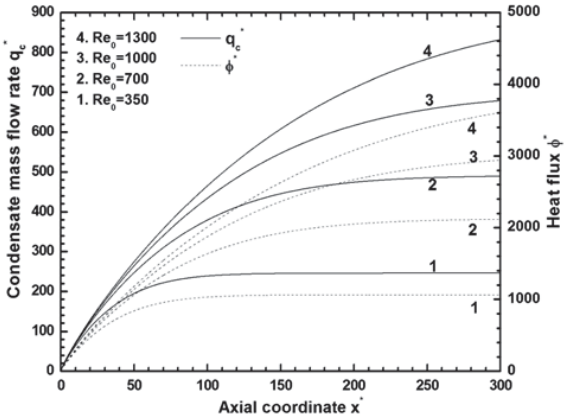

Figure 5: Effect of Re_0 on the condensation process

The same figure shows also that the axial slopes of the liquid flow rate increase with Re_0. So, the wall length required for the complete condensation increases with Re_0. Moreover, the heat flux also increases with Re_0, due to higher values of the interface temperature and the thermal gradients in the porous layer.

7.3.2 Effect of the inlet relative humidity

The effect of the relative humidity of the mixture was investigated by varying φ_0 from 0.85 to 1 corresponding to vapor concentrations C_0 between 0.7 and 0.9 for $P_0 = 1atm$, $T_0 = 98.2°C$, $Re_0 = 700$, $\Delta T = 10°C$, $\theta = 5°$.

Results presented in Fig. 6 show the important effect of φ_0 on the condensation process. An increase in φ_0 affects the thermophysical properties of the mixture at the channel inlet, leading to an increase in the partial vapor pressure, the steam mass flow rate and the inlet vapor mass fraction C_0 while the final vapor concentration C_f remains constant. Therefore, the vapor concentration gradient at the interface increases significantly with φ_0. It follows a large increase of the condensation and the liquid flow rate. We also note a significant increase of the axial slopes of the curves in the entrance region, resulting in a sharp reduction of the distance required for the end of condensation. Moreover, the increase in the liquid flow rate with φ_0

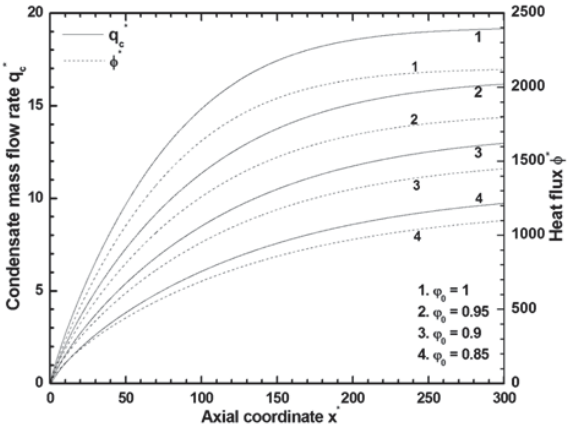

Figure 6: Effect of the inlet relative humidity on the condensation process

promotes an important enhancement of thermal flux and heat transfer at the lower cooled wall.

7.3.3 Effect of the inclination angle

The effect of the inclination angle was also analyzed for θ varying between 2 and 90° for $P_0 = 1atm$, $T_0 = 98.2^\circ C$, $\varphi_0 = 1$, $C_0 = 0.9$, $Re_0 = 700$, $T_w = 88.2^\circ C$.

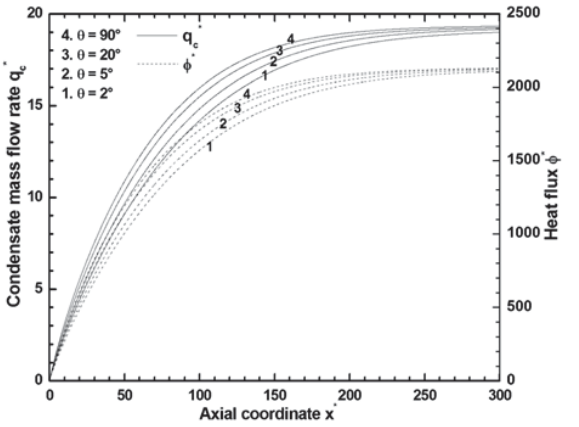

Figure 7: Effect of the inclination angle on the condensation process

From Fig. 7, we note that an increase in θ leads to an enhancement of the condensate flow rate due to an increase of liquid velocity under the effect of gravity. It

also enhances the heat flux through the wall due to a quick decrease of the interface temperature. Consequently, the wall length required for the end of condensation decreases and reaches its minimal value for the vertical case. However, the values of liquid flow rate and heat flux converge to the same final limits, because of the same initial and final state of fluids regardless of the inclination angle.

7.3.4 Effect of the porous layer properties

The effects of the porous layer properties are analyzed by varying its main properties (thickness, Darcy number, effective viscosity and effective thermal conductivity) in the following ranges: $0.0025 \leq H^* \leq 0.015$, $5 \times 10^{-6} \leq Da \leq 10^{-3}$, $0.75 \leq \mu_e^* \leq 20$, $0.5 \leq \lambda_e^* \leq 5$. The calculations are performed for $\theta = 5°$, $P_0 = 1atm$, $T_0 = 98.2°C$, $\varphi_0 = 1$, $C_0 = 0.9$, $Re_0 = 700$, $T_W = 88.2°C$. The study presented here is limited to low values of thickness H to verify the assumption that the porous layer is completely covered by the condensate at the channel inlet.

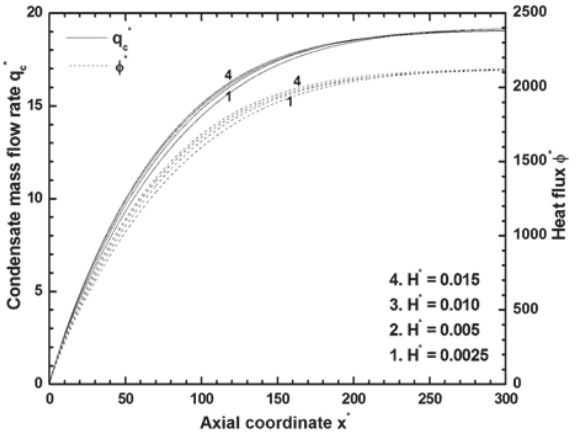

Figure 8: Effect of the porous layer thickness on the condensation process

Figures 8 and 9 represent respectively the effect of the thickness and the permeability of the porous layer on the axial developments of the condensate flow rate and the heat flux transmitted to the lower wall. These properties characterize the hydrodynamic behavior of the porous medium. Indeed, an increase in the thickness of the porous layer leads to a slight increase in the total condensate flow rate and the heat flux. These results are due to the increase in the internal pore volume in which the fluid flow occurs, leading to enhance the condensate transfer through the porous medium. Similar evolutions are also obtained with the effect of the permeability. We note that an increase in Da leads to relatively small changes on the evolutions

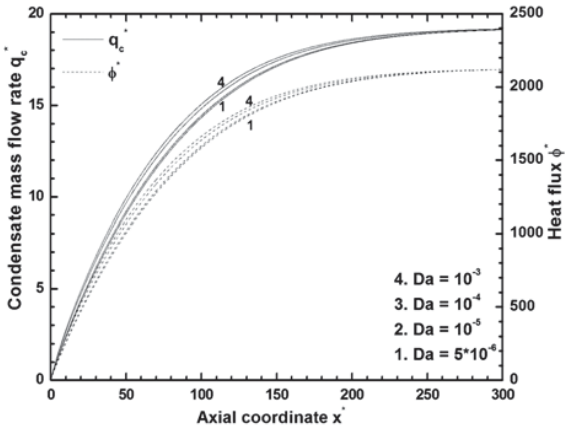

Figure 9: Effect of the Darcy number on the condensation process

of liquid flow and heat flux in the operating conditions used in this study.

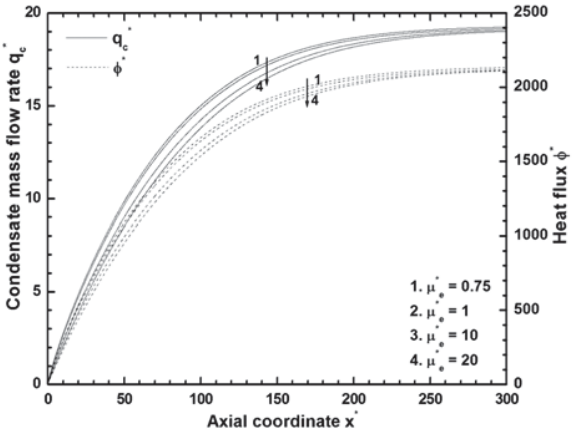

Figure 10: Effect of the effective viscosity on the condensation process

Figure 10 shows the influence of the effective viscosity of the condensate flowing in the porous layer. In fact, a major difficulty in using the Darcy-Brinkman-Forchheimer model is the evaluation of μ_e which is often assimilated to that of the fluid by most authors. Results presented in Fig. 10 show that an increase of μ_e leads to a slight decrease of the liquid flow rate and the heat flux. These evolutions can be explained by the effects of the complex geometry of porous structure and the small pore size which may hamper the liquid flow. Therefore, it behaves like a

fluid with higher effective viscosity resulting in a reduction of condensate velocity and liquid flow rate. In addition, it can be seen that the channel distance up to the end of condensation increases with μ_e.

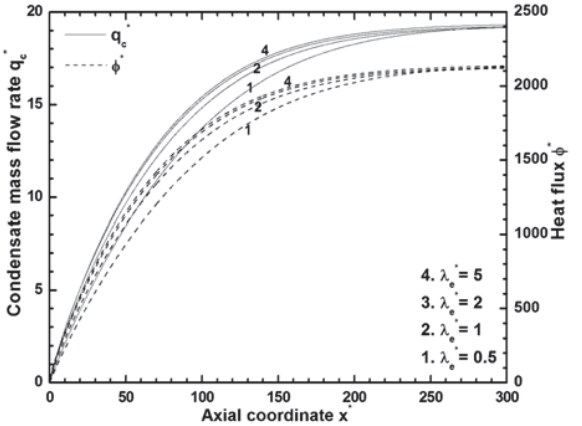

Figure 11: Effect of the effective thermal conductivity on the condensation process

Finally, Fig. 11 shows the influence of λ_e^* (representing the ratio of the thermal conductivities of the porous layer and the liquid) on the evolutions of the condensate flow rate and the heat flux. We note that its increase leads to a significant augmentation of the condensation rate, the liquid flow rate and the heat flux. Indeed, in this case, the temperature of the inner face of the porous layer decreases, resulting in an increase of concentration gradients at the liquid-mixture interface. Moreover, the heat flux produced by the condensation process is transferred by conduction through the porous wall. It follows an important effect on the evolutions of the condensation rate and the heat flux and a decrease in the wall length required for the end of condensation. However, in all cases, the limit values of the condensate flow rate and the total heat flux at the lower wall remain unchanged regardless of the porous wall properties.

8 Conclusion

We have presented a numerical study focusing on the phenomenon of laminar film condensation induced by forced convection of a steam-air mixture in an inclined channel with a saturated porous layer. The related mathematical model has been based on the proper consideration of heat and mass transport in the different phases involved. In particular, transfers in the porous layer have been modeled in the framework of the Darcy-Brinkman-Forchheimer approximation.

The resulting equations, coupled via the continuity of shear stress, heat and mass flux at the porous layer-liquid and liquid-mixture interfaces, have been solved numerically by a finite difference method based on an implicit scheme.

The calculations have been carried out over a wide range of operating conditions.

The following main conclusions have been obtained:

- The velocity in the porous layer and the liquid film increases progressively along the flow but remains much lower than that of the mixture at the end of condensation.

- In all regions of the system, the temperature and the vapor mass fraction distributions decrease gradually along the channel and tend to final values corresponding to isothermal saturation at the cooling wall temperature.

- The condensate flow rate and the wall heat flux increase significantly with the inlet Reynolds number, the inlet relative humidity and the inclination angle of the channel. However, their enhancement with the thickness, the permeability and the effective thermal conductivity of the porous layer is much smaller.

- Under the operating conditions used in this study, the wall length required to reach the end of condensation decreases with an increase in the inlet mixture relative humidity, the inclination angle of the channel and the porous layer properties.

References

Al-Ajmi, R.; Mosaad, M. (2012): Heat exchange between film condensation and porous natural convection across a vertical wall. *Fluid Dyn. Mater. Process.*, vol. 8, no. 1, pp. 51–68.

Asbik, M.; Chaynane, R.; Boushaba, H.; Zeghmati, B.; Khmou, A. (2003): Analytical investigation of forced convection film condensation on a vertical porous-layer coated surface. *Heat Mass Transfer*, vol. 40, pp. 143–155.

Asbik, M.; Zeghmati, B.; Gualous-Louahlia, H.; Yan, W. M. (2007): The effect of thermal dispersion on free convection film condensation on a vertical plate with a thin porous layer. *Transport Porous Med.*, vol. 67, no. 3, pp. 335–352.

Bories, S.; Prat, M. (1995): Transferts de chaleur dans les milieux poreux. *Techniques de l'Ingénieur*, pg. B8250.

Chaynane, R.; Asbik, M.; Boushaba, H.; Zeghmati, B.; Khmou, A. (2004): Etude de la condensation en film laminaire d'une vapeur pure et saturée sur la paroi poreuse d'une plaque incline. *Mécanique et Industries*, vol. 5, no. 4, pp. 381–391.

Choukairy, K.; Bennacer, R. (2012): Numerical and analytical analysis of the thermosolutal convection in an heterogeneous porous cavity. *Fluid Dyn. Mater. Process.*, vol. 8, no. 2, pp. 155–173.

El-Hammami, Y.; Feddaoui, M.; Mediouni, T.; Mir, R.; Mir, A. (2010): Etude numérique de la condensation en film par convection mixte à l'intérieur d'un canal à paroi poreuse. *Revue Internationale d'Héliotechnique*, vol. 42, pp. 18–24.

Hamimid, S.; Guellal, M.; Amroune, A.; Zeraibi, N. (2012): Effect of a porous layer on the flow structure and heat transfer in a square, cavity. *Fluid Dyn. Mater. Process.*, vol. 8, no. 1, pp. 69–90.

Kaviany, M. (1991): *Principles of Heat Transfer in Porous Media*. Ed. Springer-Verlag, New-York.

Labed, N.; Bennamoun, L.; Fohr, J. P. (2012): Experimental study of two-phase flow in porous media with measurement of relative permeability. *Fluid Dyn. Mater. Process.*, vol. 8, no. 4, pp. 423–436.

Lappa, M. (2004): Combined effect of volume and gravity on the three-dimensional flow instability in non-cylindrical floating zones heated by an equatorial ring. *Physics of Fluids*, vol. 16, no. 2, pp. 331–343.

Lappa, M. (2005): Thermal convection and related instabilities in models of crystal growth from the melt on earth and in microgravity: Past history and current status. *Cryst. Res. Technol.*, vol. 40, no. 6, pp. 531–549.

Lappa, M. (2007a): Secondary and oscillatory gravitational instabilities in canonical three-dimensional models of crystal growth from the melt, part2: Lateral heating and the hadley circulation. *Comptes Rendus Mécanique*, vol. 335, no. (5-6), pp. 261–268.

Lappa, M. (2007b): Secondary and oscillatory gravitational instabilities in canonical three-dimensional models of crystal growth from the melt, part1: Rayleigh-bènard systems. *Comptes Rendus Mécanique*, vol. 335, no. (5-6), pp. 253–260.

Lappa, M. (2011): Some considerations about the symmetry and evolution of chaotic rayleigh-bénard convection: The flywheel mechanism and the "wind" of turbulence. *Comptes Rendus Mécanique*, vol. 339, pp. 563–572.

Lappa, M. (2013): On the existence and multiplicity of one-dimensional solid particle attractors in time-dependent rayleigh-bénard convection. *Chaos*, vol. 23, no. 1, pp. 013105.

Ma, X.; Wang, B. (1998): Film condensation heat transfer on a vertical porous-layer coated plate. *Sci. China Ser. E*, vol. 41, no. 2, pp. 169–175.

Nield, D. A.; Bejan, A. (1998): *Convection in Porous Media*. Ed. Springer-Verlag, New-York.

Ram, P.; Bhandari, A. (2012): Flow characteristics of revolving ferrofluid with variable viscosity in a porous medium in the presence of stationary disk. *Fluid Dyn. Mater. Process.*, vol. 8, no. 4, pp. 437–452.

Renken, K. J.; Carneiro, M. J.; Meechan, K. (1994): Analysis of laminar forced convective condensation within thin porous coatings. *J. Thermophys. Heat Tr.*, vol. 8, no. 2, pp. 303–308.

Renken, K. J.; Raich, M. R. (1996): Forced convection steam condensation experiments within thin porous coatings. *Int. J. Heat Mass Transfer*, vol. 39, no. 14, pp. 2937–2945.

Renken, K. J.; Soltykiwicz, D. J.; Poulikakos, D. (1989): A study of laminar film condensation on a vertical surface with a porous coating. *Int. Commun. Heat Mass*, vol. 16, no. 2, pp. 181–192.

Shekarriz, A.; Plumb, O. A. (1989): Enhancement of film condensation using porous fins. *J. Thermophys. Heat Tr.*, vol. 3, no. 3, pp. 309–314.

Siow, E. C. (2001): *Numerical solution of a two-phase model for laminar film condensation of vapour-gas mixtures in channels*. mathesis, University of Manitoba, Canada, 2001.

Appendix A: Nomenclature

c_p	specific heat $(J.kg^{-1}.K^{-1})$
C	vapor mass fraction
D_v	diffusion coefficient $(m^2.s^{-1})$
F	Forchheimer coefficient
g	gravitational acceleration $(m.s^{-2})$
G	pressure gradient $= dP/dx(Pa.m^{-1})$
H	thickness of porous layer (m)
J_v	local mass flux $(kg.m^{-2}.s^{-1})$
K	permeability of porous coating (m^2)

L	channel length (m)
L_c	latent heat of condensation $(J.kg^{-1})$
N_k	number of nodes along η direction
$M^{'}, M$	number of nodes along x direction
M_k	molar mass of fluid k $(kg.mol^{-1})$
P	pressure (Pa)
q	mass flow rate per unit width $(kg.m^{-1}.s^{-1})$
R	plate spacing (m)
T	temperature (K)
U	velocity in the x direction $(m.s^{-1})$
V	velocity in the y direction $(m.s^{-1})$
x	coordinate along the channel (m)
y	coordinate across the channel (m)

Greek symbols

α_k	thermal diffusivity of fluid k $(m^2.s^{-1})$
δ	condensate thickness (m) (porous layer and liquid film)
$\Delta\eta_k$	transverse grid spacing in fluid k
Δx_i	axial grid spacing $(i = 1, 2)$
ΔT	temperature difference$= T_0 - T_w(K)$
η_k	transformed transverse coordinate
ε	porosity of porous coating
λ	thermal conductivity $(W.m^{-1}.K^{-1})$
μ	dynamic viscosity $(kg.m^{-1}.s^{-1})$
υ	kinematic viscosity $(m^2.s^{-1})$

ρ density ($kg.m^{-3}$)

θ angle of declination (rad)

φ relative humidity

Dimensionless parameters

Da Darcy number

Nu Nusselt number

Re Reynolds number

γ ratio of molar masses

λ_e^* ratio of thermal conductivities

μ_e^* ratio of dynamic viscosities

ϕ^* total heat flux at the wall

Subscripts and superscripts

$*$ dimensionless quantity

0 at the inlet ($x = 0$)

a air

c condensate

e effective (porous layer)

f end of condensation process

i liquid-mixture interface

k phase (liquid, mixture, porous layer)

L liquid

M vapor-gas mixture

P porous layer

v vapor

w at the lower wall